

## Stabilization of nonlinear lattices: A route to superfluidity and hysteresis

Gentaro Watanabe<sup>1,\*</sup> and Yongping Zhang<sup>2,†</sup><sup>1</sup>*Department of Physics and Zhejiang Institute of Modern Physics, Zhejiang University, Hangzhou, Zhejiang 310027, China*<sup>2</sup>*Department of Physics, Shanghai University, Shanghai 200444, China*

(Received 26 January 2018; published 24 July 2018)

The Bloch states of Bose-Einstein condensates (BECs) in pure nonlinear lattices (NLs) are dynamically unstable so that they cannot show superfluidity. We overcome this problem by finding that the two-component BECs in NLs can be stabilized by coherent linear coupling. Furthermore, in the limit of strong coherent coupling, the lowest Bloch band in the whole Brillouin zone can be dynamically stable. We also find a hysteretic behavior with looplike structure in the Bloch band resembling the so-called “swallowtail” loop. The dynamical stabilization and the looplike band structure can be realized in experiments by current technology. Our results are obtained from a discrete model, and major results are also confirmed by a continuum model.

DOI: [10.1103/PhysRevA.98.013625](https://doi.org/10.1103/PhysRevA.98.013625)

### I. INTRODUCTION

Understanding and controlling nonlinear phenomena is a profound issue in various areas of natural sciences. However, such programs often end up with difficulty because of the lack of controllability required to tune the system parameters. Recent development of the experimental techniques of cold atomic gases [1] and nanophotonics [2] is changing the situation, which allows us to realize highly controllable nonlinear systems. In cold atomic gases, the strength of the nonlinearity can be controlled by the Feshbach resonance [3]. Currently, even fine control of the strength with high spatial resolution at the submicron scale is possible [4] using the optical Feshbach resonances [5]. Although the optical Feshbach resonances suffered from strong inelastic losses in early experiments [6,7], various new techniques allow optical control of the strength with low loss rate [8–14], leading to longer sample lifetime up to the order of 100 ms [15–17]. In photonics, nonlinearity can be introduced by Kerr media, and recent nanofabrication techniques enable us to make nonlinear media with various fine structures [18].

Nonlinear lattices (NLs) are the novel setup recently realized in the above highly controllable nonlinear systems [19]. There, the periodicity of the system is set by the nonlinear term instead of the linear external potential, unlike ordinary crystalline lattices. In Bose-Einstein condensates (BECs) of ultracold atomic gases, this can be achieved by periodically modulating in space the coefficient of the nonlinear term using, e.g., an optical Feshbach resonance [4,5]. For electromagnetic waves, NLs can be realized using photonic crystals with alternating layers of different nonlinear media [20]. There is ongoing active research on various nonlinear objects such as solitons and vortices in NLs (e.g., [2,19] and references therein).

Nevertheless, the study of NLs is facing a crucial challenge: even at zero superflow, we cannot keep the lowest stationary

periodic states in NLs because of the dynamical instability unless we introduce a sufficiently large uniform repulsive interaction coefficient [21]. Therefore, almost all experimental studies of the NL so far are limited to the above-mentioned localized nonlinear objects. Stabilizing the lowest extended periodic states in pure NLs without a uniform interaction coefficient to achieve superfluidity in this system stands out as an open problem. It is worthwhile to note that stabilization of extended periodic states in various nonlinear systems is of interest in the literature, e.g., Ref. [22] for a higher branch of the stationary states, Ref. [23] for dipolar BECs in an optical lattice, and Ref. [24] for superfluid Fermi gases in an optical lattice.

In this work, we overcome this challenge using two-component BECs. We find that the pure NLs can be stabilized by an interspecies, coherent linear coupling. In particular, the lowest branch can be dynamically stable in the whole Brillouin zone (BZ) in the limit of strong coherent coupling, which cannot be achieved by simply introducing the uniform and positive interaction coefficient. We also find that this system can show a hysteretic behavior with a looplike structure in the Bloch band which resembles the so-called “swallowtail” loop [25–35]. (See, e.g., Refs. [27,33] for the connection between the looplike structure in the energy dispersion and the hysteresis.)

### II. SETUP AND FORMALISM

We consider two-component BECs (labeled by component  $a$  and  $b$ ) in NLs generated by the spatially periodic intraspecies interaction strength  $g_a$  and  $g_b$ . For simplicity, we assume that the NLs are one directional, which we take to be in the  $x$  direction. We further assume that the period  $d$  of the NL and the mass  $m$  of the atoms, which is set to unity, are the same for components  $a$  and  $b$ . We introduce the coherent linear coupling between the two NLs whose energy functional  $E_{\text{CLC}}$  is given by

$$E_{\text{CLC}} = \frac{\Omega_0}{2} \int d\mathbf{r} (\Psi_a^* \Psi_b + \text{c.c.}), \quad (1)$$

\*gentaro@zju.edu.cn

†yongping11@t.shu.edu.cn

where  $\Omega_0$  is the Rabi frequency, which is set to be real, and  $\Psi_\sigma$ 's are the condensate wave functions of component  $\sigma = \{a, b\}$ .

This system can be described by the time-dependent Gross-Pitaevskii (GP) equation,

$$i\partial_t \begin{pmatrix} \Psi_a \\ \Psi_b \end{pmatrix} = \left[ \begin{pmatrix} H_a & 0 \\ 0 & H_b \end{pmatrix} + \frac{\Omega_0}{2} \sigma_x \right] \begin{pmatrix} \Psi_a \\ \Psi_b \end{pmatrix} \equiv H_{\text{GP}} \psi, \quad (2)$$

with  $\psi \equiv (\Psi_a, \Psi_b)^\top$ ,  $\sigma_x$  being the Pauli matrix, and

$$H_\sigma \equiv -\frac{1}{2}\partial_x^2 + g_\sigma(x)|\Psi_\sigma|^2 + g_{ab}|\Psi_{\bar{\sigma}}|^2, \quad (3)$$

where  $\bar{\sigma} = \{b, a\}$  for  $\sigma = \{a, b\}$ . Here,  $g_\sigma(x) = g_\sigma^{(0)} + \frac{\Delta g_\sigma}{2} \cos(2k_0x)$  with  $k_0 = \pi/d$ , and  $g_{ab}$  is the interspecies interaction strength. The two NLs are in phase (out of phase) when  $\Delta g_a$  and  $\Delta g_b$  have the same (opposite) sign. Since one of our main purposes is to show that the pure NLs without the uniform component of the interaction strength can be stabilized, we set  $g_\sigma^{(0)} = 0$  hereafter.

This setup could be mapped to a simplified discrete model [36,37]: reducing the system with a spatially periodic interaction strength in the continuum representation to a discrete representation by sampling just two points per period of the interaction strength (the maxima and minima of the interaction strength). Thus in this discrete model, the spacing between two neighboring sites is  $\tilde{d} = d/2$ . In this representation, the on-site interaction parameter alternates between  $U_\sigma$  and  $-U_\sigma$  ( $\sigma = \{a, b\}$ ) at the adjacent sites. Assuming that the hopping parameter  $K$  is equal between components  $a$  and  $b$ , the Hamiltonian is written as

$$H = \sum_{\sigma=\{a,b\}} \sum_j \left[ -K(c_{\sigma,j}^* c_{\sigma,j+1} + \text{c.c.}) + (-1)^j \frac{U_\sigma}{2} |c_{\sigma,j}|^4 \right] + \frac{U_{ab}}{2} \sum_j |c_{a,j}|^2 |c_{b,j}|^2 + \frac{\Omega}{2} \sum_j (c_{a,j}^* c_{b,j} + \text{c.c.}), \quad (4)$$

where  $c_{\sigma,j}$  is the amplitude of component  $\sigma$  at site  $j$ ,  $U_{ab}$  is the intercomponent interaction parameter, and  $\Omega$  is the Rabi coupling constant. The discrete model has been used in the previous studies of superflow in NLs [36,37], which have demonstrated that the model can capture well the qualitative properties of the extended states of BECs in NLs, including their stability. Furthermore, we have confirmed that the discrete model can describe well the key features of the present system obtained from the full continuum model as well.

Equations of motion (EOMs) in the discrete model are given by the Euler-Lagrange equations for  $c_{\sigma,j}$  with the Lagrangian  $\mathcal{L} = \sum_\sigma \sum_j [\frac{i}{2}(c_{\sigma,j}^* \partial_t c_{\sigma,j} - c_{\sigma,j} \partial_t c_{\sigma,j}^*)] - H$ , with  $H$  given by Eq. (4). They read

$$i\dot{c}_{\sigma,j} = -K(c_{\sigma,j+1} + c_{\sigma,j-1}) + (-1)^j U_\sigma |c_{\sigma,j}|^2 c_{\sigma,j} + \frac{U_{ab}}{2} |c_{\bar{\sigma},j}|^2 c_{\sigma,j} + \frac{\Omega}{2} c_{\bar{\sigma},j}. \quad (5)$$

We consider periodic states in which  $c_{\sigma,j}$ 's are in the Bloch form:  $c_{\sigma,j} = h_{\sigma,j} \exp(ikj\tilde{d})$ , where  $k$  is the quasi-wave number of the bulk superflow [38], which is defined within the first BZ  $|k| \leq k_0$ , and  $h_{\sigma,j}$ 's are the complex amplitudes with period  $2\tilde{d}$ :  $h_{\sigma,j} = h_{\sigma,j+2}$ . Because of the constraint on the total number of particles  $\nu$  per unit cell consisting of two sites and the arbitrariness of the overall phase, the number of independent variables is six out of eight [real and imaginary parts for four

amplitudes  $h_{\sigma,1}$  and  $h_{\sigma,2}$  ( $\sigma = \{a, b\}$ )]. Stationary solutions of  $c_{\sigma,j} = c_{\sigma,j}^{(0)}$  are obtained by extremizing the Hamiltonian (4) under the normalization,  $\sum_\sigma (|h_{\sigma,1}|^2 + |h_{\sigma,2}|^2) = \nu$ , with respect to the six independent variables.

The stability of superfluidity can be judged by whether perturbations added to the stationary state grow in time, using the linear stability analysis (e.g., [1,39,40]). We first linearize the EOMs (5) in terms of the perturbations  $\delta c_{\sigma,j}(t)$  around the stationary solution  $c_{\sigma,j}^{(0)}$ . We consider the following general form of the perturbations for the periodic system,  $\delta c_{\sigma,j} = e^{ikj\tilde{d}-i\mu t}(u_{\sigma,j} e^{iqj\tilde{d}-i\omega t} + v_{\sigma,j}^* e^{-iqj\tilde{d}+i\omega t})$ , where  $q$  is the quasi-wave number of quasiparticles,  $\mu$  is the chemical potential of the stationary state, and the Bogoliubov quasiparticle amplitudes  $u_{\sigma,j}$  and  $v_{\sigma,j}$  have the same periodicity (period  $2\tilde{d}$ ) as the stationary solutions. Substituting  $c_{\sigma,j}(t) = c_{\sigma,j}^{(0)} + \delta c_{\sigma,j}(t)$  into the linearized EOMs, we obtain an eigenvalue equation  $\mathcal{M}\mathbf{u} = \omega\mathbf{u}$ , with  $\mathbf{u}^\top = (u_{a,1}, v_{a,1}, u_{a,2}, v_{a,2}, u_{b,1}, v_{b,1}, u_{b,2}, v_{b,2})$  and  $\mathcal{M}$  being an  $8 \times 8$  matrix.

It is noted that  $\mathcal{M}$  is not Hermitian and thus its eigenvalues  $\omega$  are complex in general. The condition for dynamical stability is that all the eigenvalues are real for any  $q$ . A mode corresponding to  $\omega$  with the maximum nonzero absolute value of the imaginary part is the fastest-growing mode.

In the following, we focus on the case with  $|U_a| = |U_b|$ .

### III. RESULTS

First, we discuss the lowest stationary periodic states without superflow (i.e.,  $k = 0$ ). They are obtained by numerically solving the time-independent GP equation for the Hamiltonian (4). There are two possible types of solutions both in the in-phase and out-of-phase cases: (1) polarized states with  $\nu_a \neq \nu_b$  and (2) unpolarized states with  $\nu_a = \nu_b$ , where  $\nu_a$  and  $\nu_b$  are the number of particles of  $a$  and  $b$  component per unit cell. The polarized and unpolarized states reduce to the immiscible and miscible states, respectively, in a mixture of two-component BECs corresponding to the limit of  $\Omega = 0$ . With increasing  $\Omega$ , the two components are coherently "mixed" and thus the unpolarized state starts to be favored over the polarized state at sufficiently large  $\Omega$ .

It is worthwhile to mention the behavior of the lowest stationary states in the large  $\Omega$  limit, where the lowest stationary states are unpolarized. In the out-of-phase case, the lowest stationary states lose the spatial modulation in this limit. More interestingly, in the in-phase case, if  $g_a = g_b$ , the condensate wave function of the lowest stationary state is independent of  $\Omega$ , although its stability changes according to the value of  $\Omega$ . This can be understood from the fact that the Hamiltonian  $H_{\text{GP}}$  in Eq. (2) is invariant under the combined operation of  $\sigma_x$  and exchanging  $a$  and  $b$  component because  $|\Psi_a| = |\Psi_b|$ . Therefore, the  $\Omega_0$  term in Eq. (2) can be gauged away, provided the lowest state is unique up to the overall phase.

Now we discuss the dynamical stability of the lowest stationary states without superflow (i.e.,  $k = 0$ ). Figure 1 shows the results of the linear stability analysis for the lowest periodic stationary state at  $k = 0$  plotting the maximum absolute value of the imaginary part of  $\omega$ . In the violet regions, all the eigenvalues  $\omega$  are real; if all of  $\omega$  are real at any quasimomentum  $q$  of excitations for a given  $\Omega$ , the system is dynamically stable at

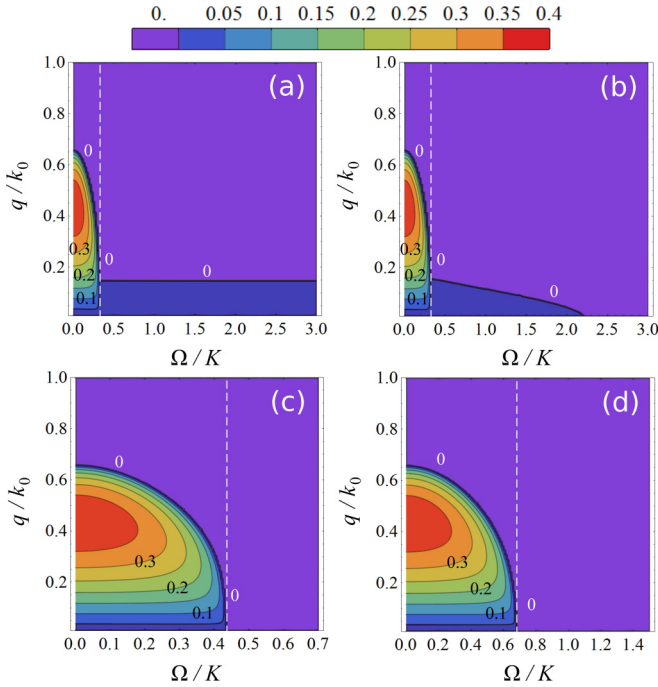


FIG. 1. Dynamical stability diagrams of the lowest stationary states at  $k = 0$  in the coherently coupled NLs. The top panels are for the in-phase (a) and out-of-phase (b) cases at  $U_{ab}v/K = 0.5$ . The bottom panels are for the out-of-phase case at  $U_{ab}v/K = 1$  (c) and 2 (d). Here, we set  $|U_{\sigma}|v/K = 1$ . The contours show the growth rate of the fastest-growing mode: the maximum absolute value of the imaginary part of the eigenvalues of the matrix  $\mathcal{M}$  in units of  $K$ . The vertical dashed line shows the boundary of  $\Omega$  below (above) which the lowest state is a polarized (unpolarized) one.

this  $\Omega$ . In both cases of in-phase and out-of-phase NLs, when  $\Omega$  is sufficiently small, the lowest state at  $k = 0$  is a polarized state, while above some threshold value of  $\Omega$  (shown by the vertical white dashed lines), the polarized state no longer exists at  $k = 0$  and an unpolarized state becomes the lowest state.

Figures 1(b)–1(d) demonstrate that the NLs could be stabilized by linear coherent coupling with large  $\Omega$ . A striking difference between the in-phase and the out-of-phase cases is that the out-of-phase NLs can always be stabilized by setting  $\Omega$  large enough while the in-phase NLs cannot be for smaller values of  $U_{ab}$  [41]. This difference can be clearly seen from the top two panels, (a) in-phase case and (b) out-of-phase case. For larger values of  $U_{ab}$ , an unpolarized state becomes dynamically stable when it becomes the lowest state due to the disappearance of a polarized state at  $k = 0$  [Figs. 1(c) and 1(d)]. In this regime, the stability diagrams of the in-phase and the out-of-phase cases are almost identical.

The transition from a dynamically unstable stationary state to a dynamically stable one can be clearly seen in their time evolution. To demonstrate this, here we use a large system with 100 unit cells (site  $j = 1-200$ ) with periodic boundary conditions. Starting from the lowest stationary state at  $k = 0$  with small random perturbations [relative magnitude is  $O(1)\%$ ] of the amplitudes  $h_{\sigma,j}$  added to the first site  $j = 1$ , we solve a set of EOMs (5) for  $j = 1-200$ . The left and the right panel of Fig. 2 show the time evolution of the populations  $|h_{\sigma,j}|^2$

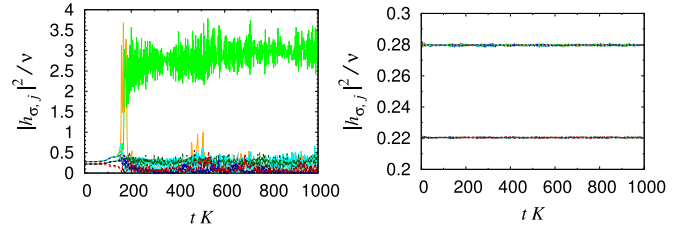


FIG. 2. Time evolution of the populations  $|h_{\sigma,j}|^2$  ( $\sigma = a$  and  $b$ ) in the first three unit cells of the out-of-phase NLs at  $|U_a|v/K = |U_b|v/K = 1$  and  $U_{ab}v/K = 1$  whose boundary between the dynamically stable and unstable regions is located at  $\Omega/K \simeq 0.43$  for  $k = 0$  [see Fig. 1(c)]. The left panel is for  $\Omega/K = 0.42$  (dynamically unstable region) and the right one is for  $\Omega/K = 0.44$  (dynamically stable region). The initial condition is the lowest stationary state at  $k = 0$  with random perturbations of order 1% of the amplitudes  $h_{\sigma,j}$  added to the first site  $j = 1$ . We use NLs with 100 unit cells with periodic boundary conditions.

of the first three unit cells in the dynamically unstable region at  $\Omega/K = 0.42$  and the dynamically stable region at  $\Omega/K = 0.44$ , respectively, in the out-of-phase NLs with  $|U_a|v/K = |U_b|v/K = 1$  and  $U_{ab}v/K = 1$  [same case as Fig. 1(c)].

We next discuss the energy band structure of the coherently coupled NLs. Figure 3 shows the energy per particle  $E_{\text{cell}}/v$  calculated from Eq. (4) as a function of  $k$ . For small  $\Omega/K$ , in both the cases of in-phase and out-of-phase NLs, the polarized branch extends the whole first BZ [the dark green line in (a)

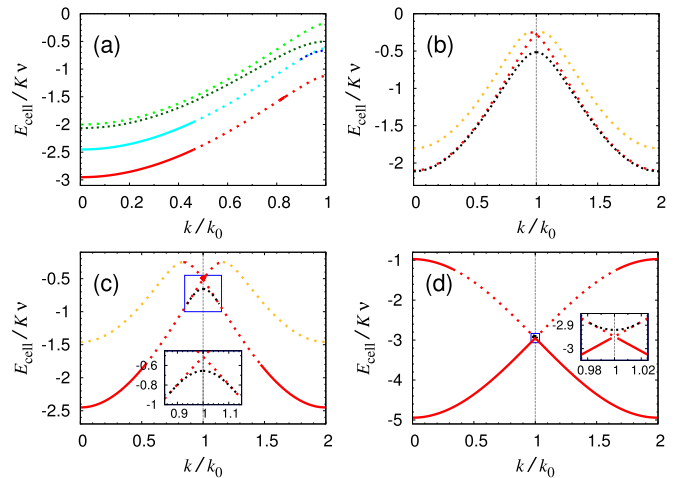


FIG. 3. Energy band for the in-phase (a) and out-of-phase (b)–(d) NLs for various  $\Omega/K$ . We set  $|U_{\sigma}|v/K = U_{ab}v/K = 1$ . In (a), the green and the dark green lines are for  $\Omega/K = 0.1$ , the cyan and the blue lines are for  $\Omega/K = 1$ , and the red line is for  $\Omega/K = 2$ . The dark green and the blue (densely dotted) lines are for the polarized branch and the others are for the unpolarized branch. In (b)–(d),  $\Omega/K = 0.3$  (b), 1 (c), and 6 (d). In these three panels, the black (densely dotted) line is for the polarized branch, the red line is for the lowest unpolarized branch, and the orange line is for the second lowest unpolarized branch. The inset of (c) and (d) is a magnification of the looplike structure around  $k/k_0 = 1$  whose domain is shown by the blue rectangle. In all panels, the solid line corresponds to the dynamically stable states and the dotted line (both the densely and loosely dotted) to the dynamically unstable ones.

and the black line in (b)] and is lower in energy compared to the unpolarized branch [the light green line in (a) and the red line in (b)]. For larger  $\Omega/K$ , the polarized states start to disappear from the BZ center ( $k = 0$ ) and the region of  $k$  of the polarized branch becomes narrower [the blue line in (a) and the black line in (c)]. Consequently, the unpolarized state becomes the lowest in energy in the region of  $k$  where the polarized states have disappeared. Note that the unpolarized states can be dynamically stable at sufficiently large  $\Omega/K$  while the polarized states are always dynamically unstable. In the in-phase case, the polarized branch completely disappears at sufficiently large  $\Omega/K$ , while in the out-of-phase case, it remains to exist around the BZ edge at  $k/k_0 = 1$  and finally becomes higher in energy compared to the lowest unpolarized branch [the inset of (d)]. Remarkably, in the limit of large  $\Omega/K$ , the lowest branch in the out-of-phase NLs is dynamically stable in the whole BZ, as can be seen from the red solid line in (d).

In out-of-phase NLs, the lowest unpolarized branch shows the overshooting behavior with respect to changing  $k$  such that the dispersion with the positive slope persists beyond the first BZ edge at  $k = k_0$  [the red lines in (b)–(d)], unlike the standard form of the Bloch band as in the in-phase case [panel (a)], which has zero slope at  $k = k_0$ . Together with the polarized branch [the black lines in (b)–(d)], the overshooting unpolarized branch forms a looplike band structure similar to the so-called “swallowtail” loop [25–35]. What is different from the swallowtail loop in the ordinary periodic potential is that the hysteresis loop appears at infinitesimally small values of the coefficients  $|U_\sigma|v/K$  and  $U_{ab}v/K$  of the nonlinear terms for any given nonzero  $\Omega$ .

Interestingly, the lowest and the second lowest unpolarized branches connect with each other as if they as a whole look like a single band with an enlarged BZ of  $|k| \leq 2k_0$  [the red and the orange lines in Figs. 3(b) and 3(c)]. This is because  $|\Psi_a(x)| = |\Psi_b(x \pm d/2)|$  in the unpolarized states in the out-of-phase NLs with  $|\Delta g_a| = |\Delta g_b|$  (i.e.,  $|U_a| = |U_b|$ ), and thus  $H_{\text{GP}}$  in Eq. (2) is invariant under the combined operation of the translation by half of the lattice constant and  $\sigma_x$  operation. At sufficiently large  $\Omega/K$ , the lowest unpolarized branch extends over the whole first and second BZs and, as a consequence, the second lowest unpolarized branch disappears [panel (d)].

The physical mechanism of the emergence of the overshooting and the hysteresis in the out-of-phase NLs can be understood as follows. Introducing the phase  $\theta_\sigma$  of the condensate wave function  $\Psi_\sigma$  as  $\Psi_\sigma = \sqrt{n_\sigma} e^{i\theta_\sigma}$ ,  $E_{\text{CLC}}$  can be written as  $E_{\text{CLC}} = \Omega_0 \int d\mathbf{r} \sqrt{n_a n_b} \cos(\theta_a - \theta_b)$ . Since  $|\theta_a - \theta_b| = \pi$  in the lowest unpolarized branch,  $E_{\text{CLC}} = -\Omega_0 \int d\mathbf{r} \sqrt{n_a n_b}$ . Therefore,  $E_{\text{CLC}}$  tends  $n_a$  and  $n_b$  to be equal at every site when  $\Omega_0$  is large and positive, namely,  $E_{\text{CLC}}$  with positive  $\Omega_0$  has an effect of locking densities of  $a$  and  $b$  components with each other. In the out-of-phase NLs, this effect prevents the condensate wave functions from having a node, which is necessary to render the slope of the dispersion to vanish at the first BZ edge and the overshooting appears as a result.

Finally, we discuss the experimental feasibility of our system using the realistic full continuum model given by Eq. (2). Here we take parameter values from the experiment of Ref. [4]. Following this experiment, we consider  $^{174}\text{Yb}$  atoms in NLs created by the lattice laser with the wavelength  $\lambda = 555.8$  nm (i.e.,  $d = \lambda/2 = 277.9$  nm and  $k_0 = 2\pi/\lambda = 0.01130$  nm $^{-1}$ ).

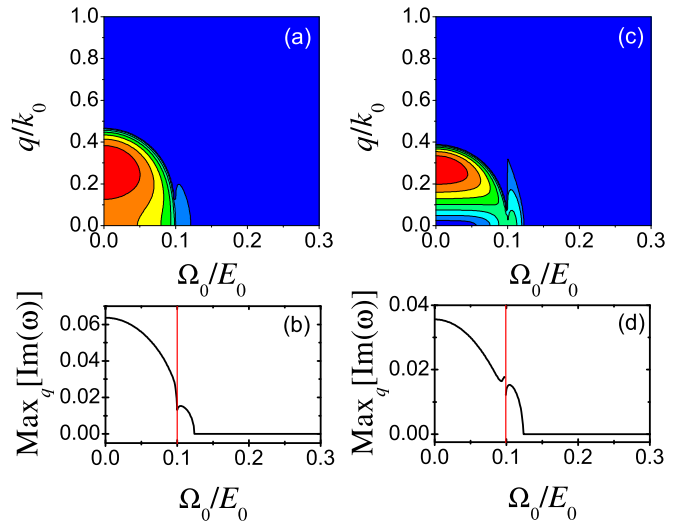


FIG. 4. Dynamical stability diagrams of the lowest stationary states at  $k = 0$  for the continuum model: (a, b) in-phase case and (c, d) out-of-phase case. Similarly to Fig. 1, (a) and (c) show the growth rate of the fastest-growing mode in units of  $E_0$ , and (b) and (d) show its maximum value with respect to  $q$ . The red vertical line in (b) and (d) shows the boundary of  $\Omega_0$  below (above) which the lowest state is a polarized (unpolarized) one.

We set the variation of the intraspecies scattering length  $\Delta a_\sigma$  of species  $\sigma$  as  $|\Delta a_\sigma| = |\Delta a_a| = |\Delta a_b| = 20$  nm, the interspecies scattering length  $a_{ab} = 5.55$  nm, and the average atom density  $n = 1.5 \times 10^{14}$  cm $^{-3}$ . Therefore, the parameters in Eq. (2) are  $|\Delta g_\sigma|n/E_0 \equiv (4\pi|\Delta a_\sigma|/m)n/E_0 = 0.3$  and  $g_{ab}n/E_0 \equiv (4\pi a_{ab}/m)n/E_0 = 0.082$ , with the energy unit  $E_0 \equiv k_0^2/m = 2\pi \times 7.4$  kHz.

The dynamical stability diagrams for the continuum model with these parameter values are shown in Fig. 4. This figure confirms the stabilization of NLs by an interspecies and coherent coupling obtained by the discrete model also holds for the continuum model [43]. We see that the NLs become dynamically stable for  $\Omega_0/E_0 \gtrsim 0.1$  in both the in-phase and out-of-phase cases. This magnitude of the Rabi frequency is easy to realize in current experiments.

In addition, stable NLs can be adiabatically prepared within a reasonable time scale of  $\gtrsim 1$  ms. Figure 5 shows the time evolution of the population obtained from the discrete model when the NLs are linearly ramped with various ramping times  $T_{\text{ramp}}$ . Parameters of the discrete model ( $U_\sigma v/K$ ,  $U_{ab}v/K$ ,  $\Omega/K$ , and  $K/E_0$ ) corresponding to the above realistic setup can be uniquely determined by fitting the intraspecies and interspecies interaction energies  $E_{\text{CLC}}$  and the effective mass of the continuum model. Results shown in Fig. 5 correspond to  $\Omega_0/E_0 = 0.2$  [44]. We consider two protocols to ramping the pure NLs with  $g_\sigma^{(0)} = 0$ : (1) starting from a uniformly repulsive intraspecies interaction with the same value as  $g_{ab}$  and (2) starting from no intraspecies interaction. While Fig. 5 shows the result of the first protocol to realize the out-of-phase NLs, there is no significant difference between the results of the two protocols. According to Fig. 5, the case of  $T_{\text{ramp}} \simeq 1$  ms is already close to the adiabatic limit. The results for ramping the in-phase NLs are also similar.

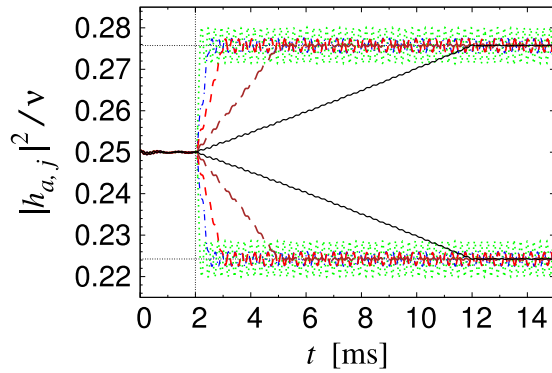


FIG. 5. Time evolution of the population of component  $a$  at the first and the second sites when the out-of-phase NLs are linearly ramped. We use NLs with 100 unit cells with periodic boundary conditions. The ramping time  $T_{\text{ramp}}$  is 0.2 ms (green dotted), 0.5 ms (blue dashed-dotted), 1 ms (red short dashed), 3 ms (brown long dashed), and 10 ms (black solid).

#### IV. CONCLUSION

We have found that the dynamical instability of the BEC in NLs can be overcome using the coherent linear coupling between two components. Especially, in out-of-phase NLs, the lowest band in the whole BZ becomes dynamically stable in

the limit of the strong coherent coupling. Since the dynamical instability of NLs has been a serious obstacle preventing us from realizing the extended states in pure NLs, it is expected that our results would provide a breakthrough to open up various experimental studies of BECs in NLs. In addition, in out-of-phase NLs, the coherent linear coupling can generate the exotic energy band structure with a hysteresis loop. Our results would also stimulate research on multicomponent systems of relevant fields such as cold gases and nanophotonics. Since the stabilization of NLs has been shown to be realized by current technology, further research on the superfluidity, transport properties, etc. and various applications of the NLs are awaited.

#### ACKNOWLEDGMENTS

We thank B. Prasanna Venkatesh and Qijin Chen for discussions. G.W. was supported by NSF of China (Grant No. 11674283), by the Fundamental Research Funds for the Central Universities (Grants No. 2017QNA3005 and No. 2018QNA3004), by the Zhejiang University 100 Plan, and by the Thousand Young Talents Program of China. Y.Z. was supported by the NSF of China (Grant No. 11774219), by the Thousand Young Talents Program of China, and by the Eastern Scholar and Shuguang (Grant No. 17SG39) Program of Shanghai.

- 
- [1] C. J. Pethick and H. Smith, *Bose-Einstein Condensation in Dilute Gases*, 2nd ed. (Cambridge University Press, New York, 2008).
  - [2] F. Lederer, G. I. Stegeman, D. N. Christodoulides, G. Assanto, M. Segev, and Y. Silberberg, *Phys. Rep.* **463**, 1 (2008).
  - [3] C. Chin, R. Grimm, P. Julienne, and E. Tiesinga, *Rev. Mod. Phys.* **82**, 1225 (2010).
  - [4] R. Yamazaki, S. Taie, S. Sugawa, and Y. Takahashi, *Phys. Rev. Lett.* **105**, 050405 (2010).
  - [5] P. O. Fedichev, Yu. Kagan, G. V. Shlyapnikov, and J. T. M. Walraven, *Phys. Rev. Lett.* **77**, 2913 (1996).
  - [6] M. Theis, G. Thalhammer, K. Winkler, M. Hellwig, G. Ruff, R. Grimm, and J. H. Denschlag, *Phys. Rev. Lett.* **93**, 123001 (2004).
  - [7] G. Thalhammer, M. Theis, K. Winkler, R. Grimm, and J. H. Denschlag, *Phys. Rev. A* **71**, 033403 (2005).
  - [8] R. Ciuryło, E. Tiesinga, and P. S. Julienne, *Phys. Rev. A* **71**, 030701(R) (2005).
  - [9] T. Zelevinsky, M. M. Boyd, A. D. Ludlow, T. Ido, J. Ye, R. Ciuryło, P. Naidon, and P. S. Julienne, *Phys. Rev. Lett.* **96**, 203201 (2006).
  - [10] K. Enomoto, K. Kasa, M. Kitagawa, and Y. Takahashi, *Phys. Rev. Lett.* **101**, 203201 (2008).
  - [11] D. M. Bauer, M. Lettner, C. Vo, G. Rempe, and S. Dürr, *Nat. Phys.* **5**, 339 (2009).
  - [12] D. M. Bauer, M. Lettner, C. Vo, G. Rempe, and S. Dürr, *Phys. Rev. A* **79**, 062713 (2009).
  - [13] M. Yan, B. J. DeSalvo, B. Ramachandran, H. Pu, and T. C. Killian, *Phys. Rev. Lett.* **110**, 123201 (2013).
  - [14] Z. Fu, P. Wang, L. Huang, Z. Meng, H. Hu, and J. Zhang, *Phys. Rev. A* **88**, 041601(R) (2013).
  - [15] S. Blatt, T. L. Nicholson, B. J. Bloom, J. R. Williams, J. W. Thomsen, P. S. Julienne, and J. Ye, *Phys. Rev. Lett.* **107**, 073202 (2011).
  - [16] L. W. Clark, L.-C. Ha, C.-Y. Xu, and C. Chin, *Phys. Rev. Lett.* **115**, 155301 (2015).
  - [17] M.-S. Kim, J. Lee, J. H. Lee, Y. Shin, and J. Mun, *Phys. Rev. A* **94**, 042703 (2016).
  - [18] G. P. Agrawal, *Nonlinear Fiber Optics*, 5th ed. (Academic Press, San Diego, CA, 2012).
  - [19] Y. V. Kartashov, B. A. Malomed, and L. Torner, *Rev. Mod. Phys.* **83**, 247 (2011).
  - [20] J. W. Fleischer, G. Bartal, O. Cohen, T. Schwartz, O. Manela, B. Freedman, M. Segev, H. Buljan, and N. K. Efremidis, *Opt. Express* **13**, 1780 (2005).
  - [21] S. L. Zhang, Z. W. Zhou, and B. Wu, *Phys. Rev. A* **87**, 013633 (2013).
  - [22] E. Ding, H. N. Chan, K. W. Chow, K. Nakkeeran, and B. A. Malomed, *Europhys. Lett.* **119**, 54002 (2017).
  - [23] A. Maluckov, G. Gligorić, L. Hadžievski, B. A. Malomed, and T. Pfau, *Phys. Rev. Lett.* **108**, 140402 (2012).
  - [24] S. Yoon, F. Dalfovo, T. Nakatsukasa, and G. Watanabe, *New J. Phys.* **18**, 023011 (2016).
  - [25] B. Wu, R. B. Diener, and Q. Niu, *Phys. Rev. A* **65**, 025601 (2002).
  - [26] D. Diakonov, L. M. Jensen, C. J. Pethick, and H. Smith, *Phys. Rev. A* **66**, 013604 (2002).
  - [27] E. J. Mueller, *Phys. Rev. A* **66**, 063603 (2002).
  - [28] M. Machholm, C. J. Pethick, and H. Smith, *Phys. Rev. A* **67**, 053613 (2003).
  - [29] B. T. Seaman, L. D. Carr, and M. J. Holland, *Phys. Rev. A* **72**, 033602 (2005).

- [30] Y. A. Chen, S. D. Huber, S. Trotzky, I. Bloch, and E. Altman, *Nat. Phys.* **7**, 61 (2011).
- [31] G. Watanabe, S. Yoon, and F. Dalfovo, *Phys. Rev. Lett.* **107**, 270404 (2011).
- [32] H. Y. Hui, R. Barnett, J. V. Porto, and S. Das Sarma, *Phys. Rev. A* **86**, 063636 (2012).
- [33] S. Eckel, J. G. Lee, F. Jendrzejewski, N. Murray, C. W. Clark, C. J. Lobb, W. D. Phillips, M. Edwards, and G. K. Campbell, *Nature (London)* **506**, 200 (2014).
- [34] D. Yu, W. Yi, and W. Zhang, *Phys. Rev. A* **92**, 033623 (2015).
- [35] S. B. Koller, E. A. Goldschmidt, R. C. Brown, R. Wyllie, R. M. Wilson, and J. V. Porto, *Phys. Rev. A* **94**, 063634 (2016).
- [36] G. Watanabe, B. P. Venkatesh, and R. Dasgupta, *Entropy* **18**, 118 (2016).
- [37] R. Dasgupta, B. P. Venkatesh, and G. Watanabe, *Phys. Rev. A* **93**, 063618 (2016).
- [38] Here we have assumed that the superflows of components  $a$  and  $b$  have the same  $k = k_a = k_b$ , which is required in order for the coherent coupling term of the Hamiltonian to be periodic.
- [39] B. Wu and Q. Niu, *New J. Phys.* **5**, 104 (2003).
- [40] L. P. Pitaevskii and S. Stringari, *Bose-Einstein Condensation* (Oxford University Press, New York, 2003).
- [41] This would be related to the dynamical instability of the unpolarized state in uniform systems triggered by a density mode at small values of intra- and interspecies interaction strengths [42].
- [42] E. V. Goldstein and P. Meystre, *Phys. Rev. A* **55**, 2935 (1997); C. P. Search and P. R. Berman, *ibid.* **63**, 043612 (2001); P. Tommasini, E. J. V. de Passos, A. F. R. de Toledo Piza, M. S. Hussein, and E. Timmermans, *ibid.* **67**, 023606 (2003); M. Abad and A. Recati, *Eur. Phys. J. D* **67**, 148 (2013).
- [43] We have also confirmed that the looplike band structure shown in Figs. 3(b)–3(d) can be obtained in the continuum model as well.
- [44] Parameters of the discrete model corresponding to  $|\Delta g_\sigma|n/E_0 = 0.3$ ,  $g_{ab}n/E_0 = 0.082$ , and  $\Omega_0/E_0 = 0.2$  are  $|U_\sigma|v/K = 1.07$  (1.03),  $U_{ab}v/K = 3.25$  (3.21),  $\Omega/K = 1.98$  (1.97), and  $K/E_0 = 0.102$  (0.102) for the out-of-phase (in-phase) case.